Biosensing in a microelectrofluidic system using optical whispering-gallery mode spectroscopy

Lei Huang and Zhixiong Guo[a)]
Department of Mechanical and Aerospace Engineering, Rutgers, the State University of New Jersey, Piscataway, New Jersey 08854, USA

(Received 4 April 2011; accepted 1 July 2011; published online 12 August 2011)

Label-free detection of biomolecules using an optical whispering-gallery mode sensor in a microelectrofluidic channel is simulated. Negatively charged bovine serum albumin is considered as the model protein analyte. The analyte transport in aqueous solution is controlled by an externally applied electrical field. The finite element method is employed for solving the equations of the charged species transport, the Poisson equation of electric potential, the equations of conservation of momentum and energy, and the Helmholtz equations of electromagnetic waves. The adsorption process of the protein molecules on the microsensor head surface is monitored by the resonance frequency shifts. Frequency shift caused by temperature variation due to Joule heating is analyzed and found to be negligible. The induced shifts behave in a manner similar to Langmuir-like adsorption kinetics; but the time constant increases due to the presence of the external electrical field. A correlation of the frequency shift, the analyte feed concentration in the solution, and the applied voltage gradient is obtained, in which an excellent linear relationship between the frequency shift and the analyte concentration is revealed. The applied voltage gradient enhances significantly the analyte concentration in the vicinity of the sensor surface; thus, the sensor sensitivity which has a power function of the voltage gradient with exponent 2.85 in the controlled voltage range. Simulated detection of extremely low protein concentration to the pico-molar level is carried out. © *2011 American Institute of Physics*. [doi:10.1063/1.3615237]

I. INTRODUCTION

Many different micro/nano detection methods have recently been applied to biochemical and biomedical processes monitoring and analysis. These methods can be broadly classified into two main categories: labeling methods and label-free methods. Labels can structurally and functionally interfere with an assay, leading to possible false negatives. They may not be specific and, moreover, impose additional time and cost demands. As a result, scientists are exploring novel techniques that do not require labeling of ligand or receptor and that allow virtually any complex to be screened with minimal assay development. Without the need for labels or agents, detection can be done *in situ* and in real time, taking great advantages in emerging point-of-care detecting applications. Several label-free optical techniques have been developed, such as autofluorescence,[1] confocal Raman spectroscopy,[2] optical resonance,[3] surface plasmon resonance,[4] and intracavity spectroscopy.[5]

There is an increasing awareness of micro-opto-fluidic systems (MOFS), which employ hybrid optical and microfluidic technologies in a micro environment to perform novel functionality and in-depth analysis.[6–11] MOFS can be realized via a simple integrated chip solution, combining fluid flow and optical sensor in a single microchannel, in which the fluid acts as a medium, which carries analytes such as biomolecules and chemicals in the microchannel for optical detection. In 1999, Guo *et al.*[7] proposed a rapid yet accurate optical interferometric method for

[a)]Author to whom correspondence should be addressed. Electronic mail: guo@jove.rutgers.edu. Tel.: 732-4452024.

measuring mass diffusion coefficients in microchannels with aqueous solutions within 100 s. In 2005, Leung *et al.*[8] developed a continuous flow microfluidic reactor, using a confocal Raman microscopy detector for online monitoring, and significantly reduced measurement time from 48 h to only 10 min. Cui *et al.*[9] has recently implemented an on-chip optofluidic microscopic system using the surface plasmon resonance technique to measure living *Caenorhabditis elegans* within 0.5 s. Burg *et al.*[10] has demonstrated a suspended microchannel resonator with embedded microfluidic channels for ultralow volume universal detection. As compared with conventional measurement instrument, the sample quantity in a microfluidic channel is substantially reduced. Traditionally, pressure is used in these devices to induce controllable fluid flow in microchannels. However, incorporation of a pressure pump or valve into a microchannel is challenging and restrictive in many situations. Thus, other manipulation schemes such as use of applied electric voltage[11] may be needed, leading to combined micro-opto-electro-fluidic systems (MOEFS).

Nowadays, research on whispering-gallery mode (WGM) based biosensing has attracted increasing attention, because of its extremely high sensitivity in the detection of molecules or nano-entities.[12–15] It is well known that WGM resonance frequencies depend on the effective size and refractive index of the resonator.[16–18] At a resonance, photons are trapped and internally reflected in an orbit within the resonator surface of circular shape. The resonance induces a strong evanescent wave field in the surrounding. As the photons guided by total internal reflection in the resonator circulate many times, they interact repeatedly with adsorbate on the surface of the resonator, leading to resonance frequency shifts.[12–14]

On the other side, temperature variation due to absorption of laser energy during laser scanning or pumping[19] could change resonator conditions because of the thermal expansion and thermo-optic effects.[20] Ma *et al.*[20,21] measured resonance wavelength shifts against temperature changes for different silica beads. The measured sensitivities closely match with the analytical values based on bulk material properties of silica thermal expansion and thermo-optic effect in a wide temperature range.[21]

In this paper, an optical WGM micro device is proposed to be integrated with a microelectrofluidic channel to provide a new MOEFS platform for label-free detection with high sensitivity in the universal analysis of biomolecules, proteins, DNA, or chemicals. The analyte solution flow in the microchannel is driven by an external electric potential. The whole process is coupled by the charge transport equations, the Poisson equation, the conservation of momentum equation, the energy conservation equation, and Maxwell's equations. All the governing equations are solved via the finite element method in a package. Emphasis is placed on investigating the optical resonance frequency shifts versus the analyte concentration and the applied electric potential gradient. The dynamic adsorption process detected by the sensor is revealed. The effect of Joule-heating is analyzed and examined. A sensor correlation is obtained.

II. MATHEMATIC FORMULATION

Consider a planar MOEFS structure shown in Fig. 1. The system consists of a microfluidic channel with two electrodes and an optical WGM resonator as the micro sensor. An anode electrode can be embedded inside the dielectric resonator to form an equipotential electrical field around the sensor surface. Analyte solution and buffer solution are forced into the channel from inlet ports toward the outlet port. The charged analytes are directed to the optical sensor through the electrostatic fluid flow. The WGM-based optical resonator coupled with a waveguide is integrated in a section of the microchannel. The enlarged view in Fig. 1 provides a detailed sketch of the simulation region with both the analyte transport and the sensor in which h indicates the inner width of the channel, l is the length in the simulation domain, d indicates the resonator diameter, and w is the width of the waveguide. A laser beam is focused into the waveguide. Photons at resonant frequencies tunnel from the waveguide to the micro resonator. The considered sample analyte in the present study is bovine serum albumin (BSA), a serum albumin protein that has many biochemical applications and can also be used as a nutrient in cell and microbial culture. BSA is stable and lack of effect in many biochemical reactions. The cost for preparing BSA is low.

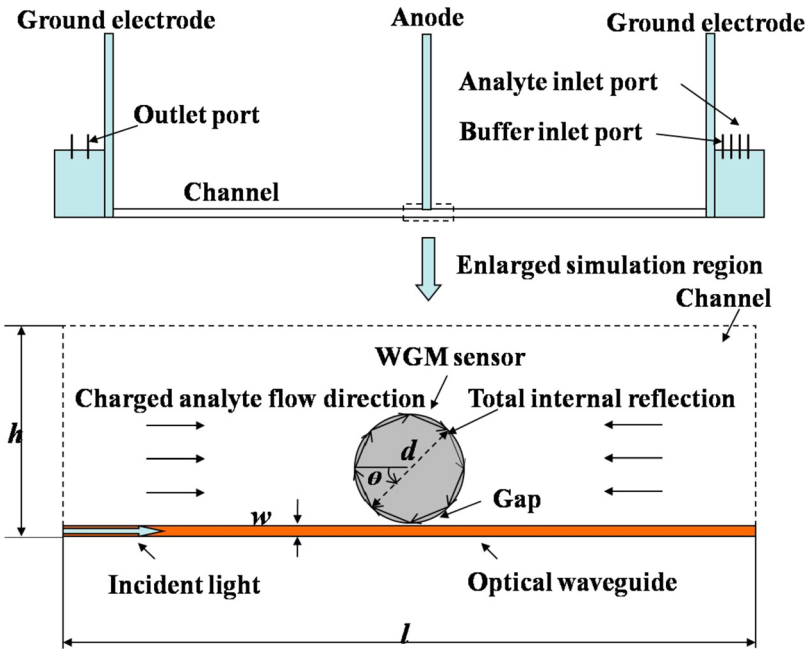

FIG. 1. Sketch of the MOEFS with a WGM sensor and the enlarged view of the simulation region.

A. Governing equations

The charge transport for analyte dissolving in pure water includes negatively charged BSA analyte, the hydroxide ions, and hydronium ions.[22] The transport equations are

$$\frac{\partial C_i}{\partial t} + \vec{V} \cdot \nabla C_i = \nabla \cdot (z_i w_i F C_i \nabla \Phi) + D_i \nabla^2 C_i, \quad i = 1, 2, 3, \tag{1}$$

where C is molar concentration; z is the valence number (in this work, we assume $z_1 = z_2 = -z_3 = -1$); w is the mobility under an external electric potential; Φ is the electric potential; D is the diffusion coefficient; and F is the Faraday constant. Subscripts $i = 1$, 2, and 3 indicate the analyte, hydroxide ion, and hydronium ion, respectively.

As the electric potential field is irrotational, it can be conveniently expressed by the following Poisson equation:

$$\varepsilon_f \nabla^2 \Phi = -\rho_E, \tag{2}$$

where

$$\rho_E = F\left(\sum_{i=1}^{3} z_i C_i\right). \tag{3}$$

Here, ρ_E is the total charge density, and ε_f is the permittivity of fluid. In the Poisson formulation, the permittivity of the solution is assumed uniform. The conductivity field is dominated by charges densities and charges' mobility is assumed constant.

The equation of conservation of momentum for the incompressible aqueous solution is

$$\frac{\partial \vec{V}}{\partial t} + \vec{V} \cdot \nabla \vec{V} = -\frac{\nabla P}{\rho} + \upsilon \nabla^2 \vec{V} - \frac{\rho_E}{\rho} \nabla \Phi, \tag{4}$$

where ρ is the liquid density, $\vec{V}$ is the velocity, P is the pressure, and υ is the dynamic viscosity. The electric potential is coupled to the momentum equation via the addition of the electric force term.

It is well known that Joule heating induced by the applied electric potential in a microelectrofluidic system may be a concern. The following heat transfer equation is employed to examine the temperature variation:

$$\rho c_p \left(\frac{\partial T}{\partial t} + \vec{V} \cdot \nabla T \right) = Q + \nabla \cdot (k \nabla T), \tag{5}$$

where $Q = \sigma |\nabla \Phi|^2$ is the Joule heat generated by the electric current flow; σ is electrical conductivity and can be defined as[22] $\sigma = F^2 (\sum_{i=1}^{3} w_i z_i^2 C_i)$ in the bulk solution; T is the temperature; ρ is the density; c_p is the heat capacity; and k is the thermal conductivity.

The micro resonator and waveguide are made of a dielectric material. The electromagnetic (EM) wave propagation and photon tunneling in the optical device can be described by time-dependent Maxwell's equations[23] as follows:

$$\nabla \cdot \vec{E} = \frac{\rho_E}{\varepsilon}, \nabla \times \vec{E} = -\mu \frac{\partial \vec{H}}{\partial t}, \tag{6}$$

$$\nabla \cdot \vec{H} = 0, \nabla \times \vec{H} = J + \varepsilon \frac{\partial \vec{E}}{\partial t}, \tag{7}$$

where $\vec{E}$ and $\vec{H}$ are the electric and magnetic field vectors, respectively; μ and J are permeability and total current density, respectively; and ϵ is the permittivity. For time-harmonic waves, $E(r,t) = E(r) exp(i\omega t)$ and ω is the angular frequency, Maxwell's equations are then simplified to the Helmholtz equations as follows:

$$\nabla^2 \vec{E} + \mu \omega^2 \varepsilon \vec{E} = 0, \tag{8}$$

$$\nabla^2 \vec{H} + \mu \omega^2 \varepsilon \vec{H} = 0. \tag{9}$$

Under WGM resonances, the EM field in a 2-D micro resonator typically consists of equatorial brilliant rings. The rings are located on the same plane as the waveguide.[14] Consider in-plane transverse electric (TE) waves, the EM fields can be simplified as

$$\vec{E}(x, y, t) = \vec{E}_z(x, y) \vec{e}_z \, e^{i\omega t}, \tag{10}$$

$$\vec{H}(x, y, t) = [\vec{H}_x(x, y) \vec{e}_x + \vec{H}_y(x, y) \vec{e}_y] e^{i\omega t}. \tag{11}$$

B. Initial and boundary conditions

In the present simulations, neutral velocity boundary conditions, which act like there were no boundaries, are assumed in the streamwise direction. Constant temperature is taken as 300 K at the outlet and inlet of the microchannel. Initial temperature is constant at 300 K as well. For the charged species, convective flux and constant concentration are adopted at the outlet and inlet of the flow, respectively. Initially, the analyte is uniformly distributed and the solution is stationary. Non-slip conditions on the walls and micro resonator surface are also assumed. The following boundary conditions are then employed on the physical walls:

$$\nabla \Phi \cdot \vec{n} = 0, \tag{12}$$

$$\nabla C_i \cdot \vec{n} = 0, \; i = 1, 2, 3, \tag{13}$$

$$\vec{V} \cdot \vec{n} = 0, \vec{V} \cdot \vec{t} = 0, \tag{14}$$

$$\vec{n} \times \vec{H} = 0, \tag{15}$$

where $\vec{t}$ and $\vec{n}$ are the tangential and normal vectors of the wall, respectively. Eqs. (12) and (13) are, respectively, the condition that the boundary is nonconductive and that there is no ion diffusion across the walls. Eq. (14) is the condition that the walls are not penetrative. Eq. (15) demonstrates the natural continuity condition for the tangential component of the magnetic field at the system interface and physical boundaries with respect to Maxwell's equations.

Protein adsorption on a solid surface is involved in a wide range of phenomena and applications and represents a complicated field of biomaterials which has been studied for decades. Under the effect of an electric potential flow, charged analytes are directed toward the oppositely charged solid surface and bind to it. On a hydrophilic surface, the electrostatic attraction between oppositely charged material is often the major driving force for adsorption of bio molecules.[24] In a Si_3N_4/H_2O solution, the neutral SiOH species becomes the predominant one, the $SiNH_3^+$ species remains the charged one, whereas the SiO^- sites increase.[25] It is known that the BSA proteins carry negative charges at neutral *p*H value.[26] To simplify the simulation work, Langmuir approach[27] is adopted to describe the protein adsorption process. The key assumptions are (a) only a monolayer forms by adsorption; (b) the adsorbing surface is composed of discrete, identical, and non-interacting sites; (c) the adsorption process for each molecule is independent; and (d) there is no molecule-molecule interactions since the concentration is very low. Moreover, with the assumption that there is no surface diffusion on the micro resonator, the boundary conditions with respect to C_i are prescribed as

$$\vec{n} \cdot (-D_1 \nabla C_1 + z_1 w_1 F C_1 \nabla \Phi + C_1 \vec{V}) = -K_{ads} C_1 (\Theta - C_s) + K_{des} C_s, \tag{16}$$

$$\nabla C_i \cdot \vec{n} = 0, \quad i = 2, 3, \tag{17}$$

Here, K_{ads} and K_{des} are the adsorption coefficient and desorption coefficient, respectively. Θ indicates the surface saturation density value when the micro resonator is fully covered by the analyte molecules. The surface density of adsorbate, C_s, is governed by

$$\frac{\partial C_s}{\partial t} = K_{ads} C_1 (\Theta - C_s) - K_{des} C_s. \tag{18}$$

It is worth mentioning that the adsorption and desorption processes only occur at the surface of the micro resonator.

As to the boundaries for the EM wave calculation domain, the low-reflecting boundary condition,[13] which indicates that only a small part of EM wave is reflected and the wave propagates through the boundary almost as if it were not present, is adopted

$$\vec{e}_z \cdot \vec{n} \times \sqrt{\mu} \vec{H} + \sqrt{\varepsilon} \vec{E}_z = 0. \tag{19}$$

The light source term $\vec{E}_{0z}$, which propagates inwards through the entry of the waveguide, can be treated as an electrically low-reflecting boundary and expressed by

$$\vec{E}_{0z} = \frac{1}{2\sqrt{\varepsilon}} (\vec{e}_z \cdot \vec{n} \times \sqrt{\mu} \vec{H} + \sqrt{\varepsilon} \vec{E}_z). \tag{20}$$

In present computations, the light source term is assumed to be uniform and unity at the entry of the waveguide.

C. Properties and parameters

In the present study, BSA with volume 224 nm and molecular weight 66 776 Da (Ref. 26) is taken as the sample analyte and pure water (pH = 7.0) as solvent. The effective refractive index of the analyte is assumed as 1.5, and each BSA molecule is assumed to take one effective negative charge. In a neutral pH 7.0 solution, the hydroxide ions and hydronium ions are in equilibrium and the ion concentration is 100 nM each at room temperature. Both the micro resonator ($d = 5$ μm) and waveguide ($w = 1$ μm) are made of silicon nitride with a bulk refractive index of 2.01. The inner width of the channel is $h = 10$ μm; and the channel length in the simulation domain is $l = 60$ μm. The electrical potential gradient is measured from the positively charged sensor surface to the ground analyte inlet. Single-mode laser with wavelength around 835 nm is used to trigger a WGM resonance inside the micro resonator through the waveguide. The gap between the micro resonator and waveguide is set at 300 nm. The extremely dilute analyte solution can be assumed to have the permittivity, viscosity, density, thermal conductivity, specific heat capacity, and refractive index of pure water.

The surface saturation concentration is taken by assuming the resonator surface is fully covered by a monolayer of BSA molecules. The reported adsorption and desorption coefficients of BSA vary, depending not only on the pH value, ionic strength, concentration, and surface conditions but also on the model used in adsorption kinetics. Since the focus of the present study is the demonstration of the WGM sensor, rather than the adsorption kinetics, the adsorption and desorption coefficients of BSA are assumed constant, close to the values given by the experiment of Yeung *et al.*[28] The property values used in the present simulation are summarized in Table I.

D. Numerical models and schemes

The current problem is very complicated and involves coupling of fluid dynamics, heat transfer, multiple species transport, electric potential distribution, and optical EM field. In the current simulation, the commercial COMSOL package (version 3.3) is applied to perform a finite element analysis. The electro-kinetics, Joule-heating, the Poisson equation, and in-plane TE waves application modes of the COMSOL package are employed and solved in coupling.

Table I. Values of parameters used in this work (at 300 K).

Symbol	Description	Value used
w_1	Mobility of BSA in water	1.5×10^{-14} mol·s/kg
w_2, w_3	Mobility of ions	5×10^{-13} mol s/kg (Ref. 32)
D_1	Diffusivity of BSA in water	3.26×10^{-11} m^2/s (Ref. 33)
D_2, D_3	Diffusivity of ions	5×10^{-9} m^2/s (Ref. 34)
K_{ads}	Adsorption coefficient of BSA	2.2 m^3/(mol·s)
K_{des}	Desorption coefficient of BSA	1×10^{-3}/s
Θ	Surface saturation concentration	4.5×10^{-8} mol/m^2
ε_f	Permittivity of water	6.93×10^{-10}C/(V·m)
ε	Permittivity of silicon nitride	3.54×10^{-11} C/(V·m)
F	Faraday constant	9.65×10^4 C/mol
ρ	Density of water	1.0×10^3 kg/m^3
υ	Viscosity of water	1.0×10^{-6} m^2/s
n_m	Refractive index of silicon nitride	2.01
n_s	Refractive index of water	1.33
n_B	Refractive index of BSA	1.5
k	Thermal conductivity of silicon nitride	30 W/(m·K)
k	Thermal conductivity of water	0.58 W/(m·K)
C_p	Specific heat capacity of silicon nitride	710.6 J/(kg·K)
C_p	Specific heat capacity of water	4.18 kJ/(kg·K)

Specifically, the electrokinetic flow mode is used to solve the charge transport equations. The Poisson equation is solved using the electrostatics mode. The fluid dynamics equations are solved using the Incompressible Navier–Stokes mode. The general heat transfer and conductive media DC modes are used to consider the Joule-heating effect. And the In-plane TE waves mode is adopted to solve Maxwell's equations.

The simulation work is generally separated into two steps: first, the charged species transport, the adsorption process, and the temperature distribution and are simulated in the domain as described in the enlarged area in Fig. 1 with 20 196 triangle elements. Locally refined meshes are applied to the vicinity around the micro resonator since attention should be paid to the adsorption of analyte on the surface of the micro resonator. All coupled modes are solved by a time-dependent solver of COMSOL with a time step of 0.1 s, and the relative tolerance is set as 10^{-6}. Second, the adsorption surface density distribution is transformed into the thickness profile of the BSA layer surrounding the resonator. The said layer together with the temperature variation will induce changes to the resonance condition of light traveling inside the micro resonator. The simulation domain for optical detection is also the enlarged area in Fig. 1 and is meshed by about 150 000 triangle elements. The existence of the thin adsorption layer (in the order of picometer) requires extremely small size of meshes in the vicinity around the periphery of the micro resonator; and hence, more refined elements are needed to perform the optical analysis. Simulations are conducted in a DELL PC with one 2.2 GHz CPU and 3.0 GB memory.

III. RESULTS AND DISCUSSION

Some previous work has shown the feasibility of applying COMSOL package to perform the analysis of molecular and fluid transport[29,30] and optical EM field.[13,14] To validate the current simulation, the adsorption of BSA at two different concentrations (20 pM and 500 pM) onto a silica micro resonator at *p*H 6.6 in the absence of external electrical field is simulated and compared with the experimental results by Yeung *et al.*[28,31] The parameter values used in the simulation were given in Table I of Yeung *et al.* through a simple Langmuir model.[28] The surface saturation concentration are calculated as 0.448×10^{-13} and 5.418×10^{-12} mol/m^2 for 20 pM and 500 pM, respectively. Figure 2 compares the time evolutions of the relative surface coverage

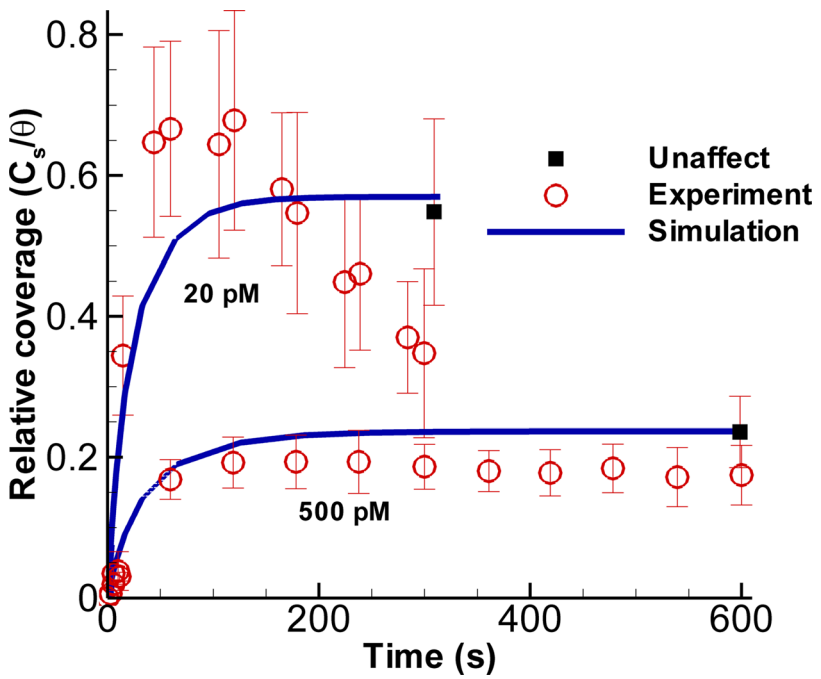

FIG. 2. Comparison between the present simulations and experiments in the literature (Refs. 28 and 31).

between the simulations and experiments. As seen, both the experimental and calculated results exhibit Langmuir-like adsorption kinetics, and the simulations agree well with the experimental measurements. It should be mentioned that the experimental results were suffered from photobleaching effect. The black solid squares at $t = 310$ and 600 s represent the relative coverage unaffected by photobleaching, from where the adsorption coefficients were obtained.[28] Thus, the simulations match excellently with the photobleaching-unaffected results; while the experimental points with photobleaching effect are generally below the simulated ones, particularly at long time stage. The experimental uncertainty is quite large for the case of extremely low concentration (20 pM). More accurate measurement techniques like the presently proposed one are in great demand.

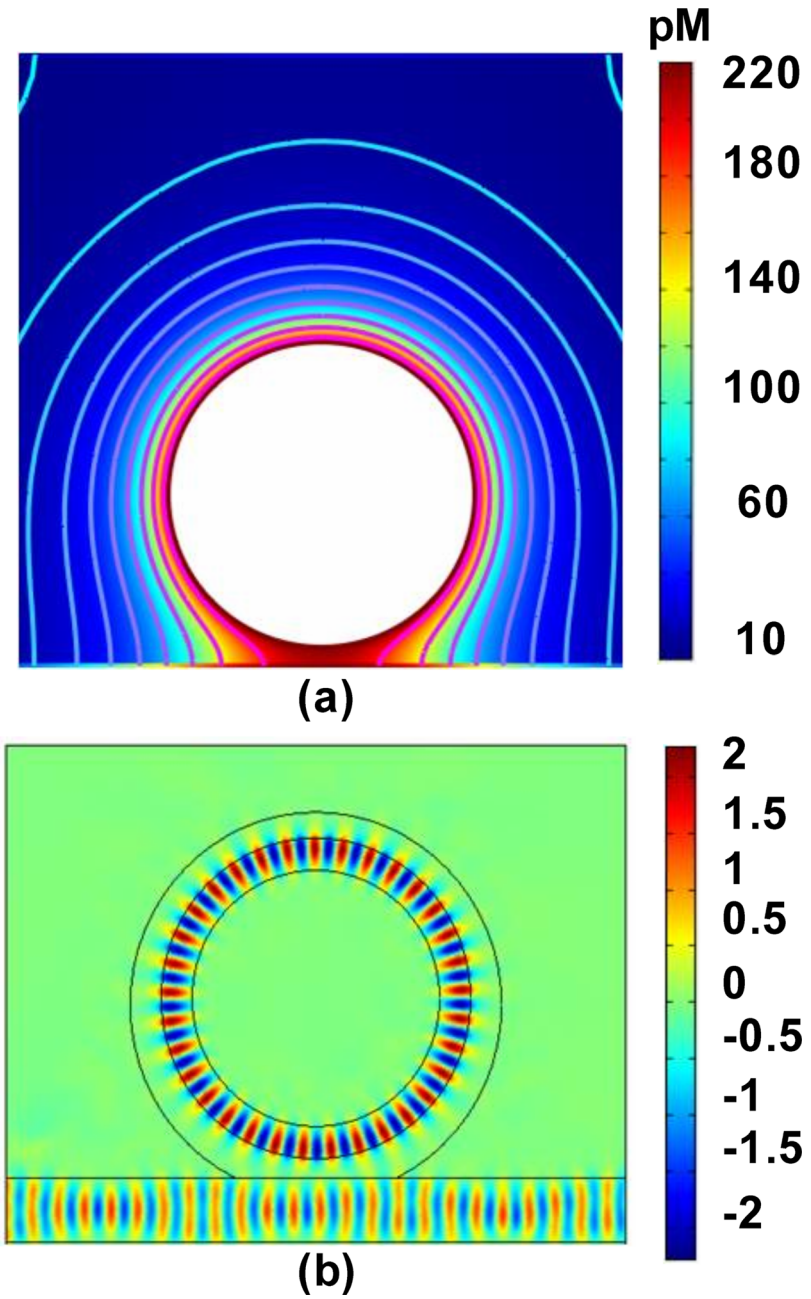

FIG. 3. Representative analyte concentration field around the sensor with electrical equipotential lines (a) and typical WGM resonance electric field under the first-order resonance (b).

Once an electric potential difference is applied to the MOEFS, samples are driven to move and some of them will be deposited at the resonator surface till the whole system reaches a new equilibrium. The monolayer formation process can be monitored by tracking the resonant frequency shift of the sensor. A typical analyte concentration distribution and a representative resonance electric field are shown in Figs. 3(a) and 3(b), respectively. In the simulation, the applied voltage gradient is 23.3 V/cm, and the BSA bulk concentration is 10 pM. Fig. 3(a) illuminates the steady-state distribution of the analyte concentration and the equipotential lines of the electrical potential field. It is seen that most of the negatively charged analytes accumulate toward the micro resonator ($d = 5$ μm) surface, which justifies the fact that in such a system, the applied electrical potential is a predominant driven mechanism over the convection and diffusion for charged analyte transport. As a result, the analyte concentration around the sensor is substantially enriched with maximum concentration about 22 times of the feed concentration, leading to augmentation of BSA adsorption on the resonator surface. The formation of adsorbed BSA monolayer varies the WGM resonance frequency. Fig. 3(b) displays the distribution of the time-varying harmonic electric field in a small region (7.75×8 μm^2) around the sensor under a first-order WGM resonance. The resonance frequency is shifted from a base frequency 178.671975 THz for the case without analyte formation to 178.671930 THz for the case with a layer of analyte formation at steady state. The analyte adsorption does not obviously degrade the resonance quality and the quality factor remains in the order of 10^4.

The steady-state distributions of the analyte density on the micro resonator surface for four different applied voltage gradients (6.67, 16.7, 23.3, and 33.3 V/cm) are shown in Fig. 4. The starting point of the θ angle is shown in Fig. 1. All simulations are performed with analyte feed concentration at 10 pM. As seen, for the cases of 6.67, 16.7, and 23.3 V/cm, the adsorbed analyte is nearly uniformly distributed on the sensor surface, and the analyte surface density increases with increasing voltage. As the applied voltage gradient increases to 33.3 V/cm, however, the analyte surface distribution becomes less uniform and the density decreases as compared with the case of 23.3 V/cm.

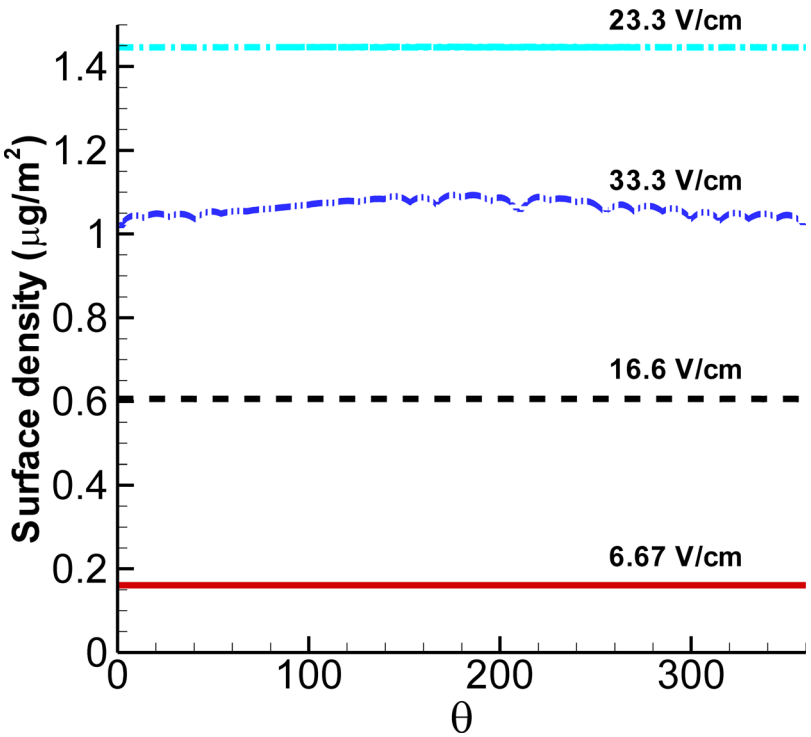

FIG. 4. The density distributions of the adsorbed analyte on the surface of micro resonator for different applied voltage gradients.

The analyte monolayer formation is a time-dependent process. Fig. 5 demonstrates the time evolution of the average surface density of the adsorbed analyte versus the applied voltage gradient. All simulations are performed with analyte feed concentration at 10 pM in neutral solution. In general, two distinct kinetic regimes can be used to describe a protein adsorption curve,[27] the transport- and adsorption-limited regimes. In this study, the negatively charged analyte flows toward the anode from an initial distribution under the external electrical effect, which is a transport-limiting mechanism. As the adsorption and desorption processes proceed, according to the monolayer assumption, surface active sites diminish, and thus, reducing the rate of adsorption and the deposition process is in the adsorption-limit regime in the vicinity around the resonator surface. When a significant fraction of the surface is covered, the rate of the analyte adsorption will be balanced by the rate of desorption and saturation is reached. The results in Fig. 5 show Langmuir-like adsorption kinetics, which follows the formula $C_s = C_{sat}\ [1 - \exp(-t/\tau)]$, in which C_{sat} is the absorbate surface density at saturation and τ is the time constant. The time constants for the four different electrical potential gradients of 6.67, 16.7, 23.3, and 33.3 V/cm are 1963, 3337, 4298, and 3398 s, respectively. The time constant increases with increasing saturation surface density C_{sat}. From Figs. 4 and 5, it is clear that for the three cases of 6.67, 16.7, and 23.3 V/cm, the analyte adsorption process is in the adsorption-limited regime.[27] For the case of 33.3 V/cm, however, the adsorption process is transport-limited.

To further inspect the influence of the applied voltage, the variations of the averaged analyte surface density at equilibrium versus the applied voltage gradient for two different feed concentrations (10 pM and 50 pM) are plotted in Fig. 6. It is seen that the analyte surface density increases as the applied voltage gradient increases up to about 26.7 V/cm and after which the analyte surface density decreases as the applied voltage gradient goes up. This is because the applied voltage increases the bulk solution flow velocity as well. When the flow velocity is increased to a value such that the convection is comparable to the electrical driven force, further increase of the applied voltage will start to reduce the enriched concentration field and the overall analyte adsorption density. Therefore, the applied voltage should be controlled in a range smaller than 26.7 V/cm.

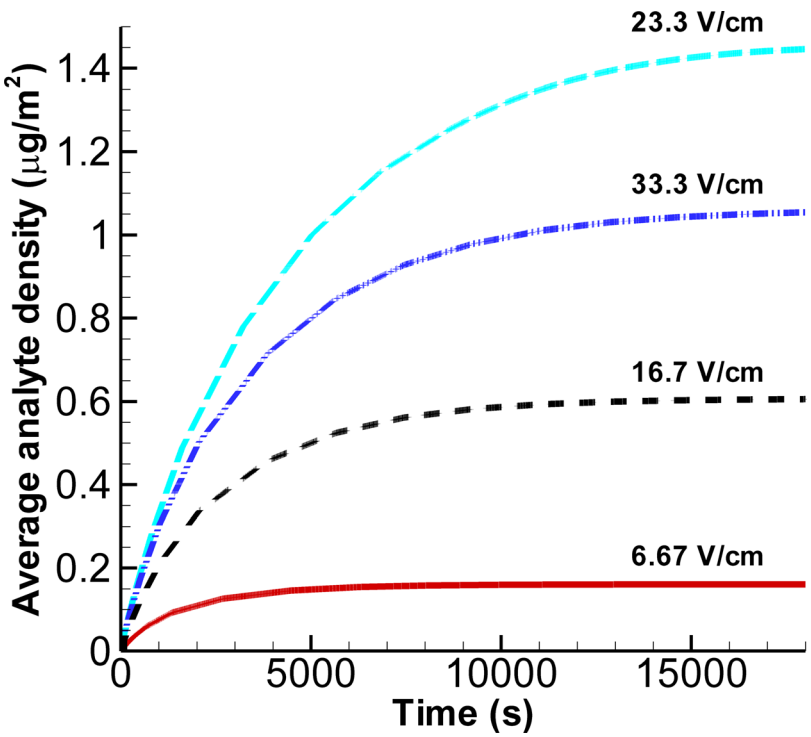

FIG. 5. The time trace of the adsorbed analyte on the micro resonator surface for different applied voltage gradients.

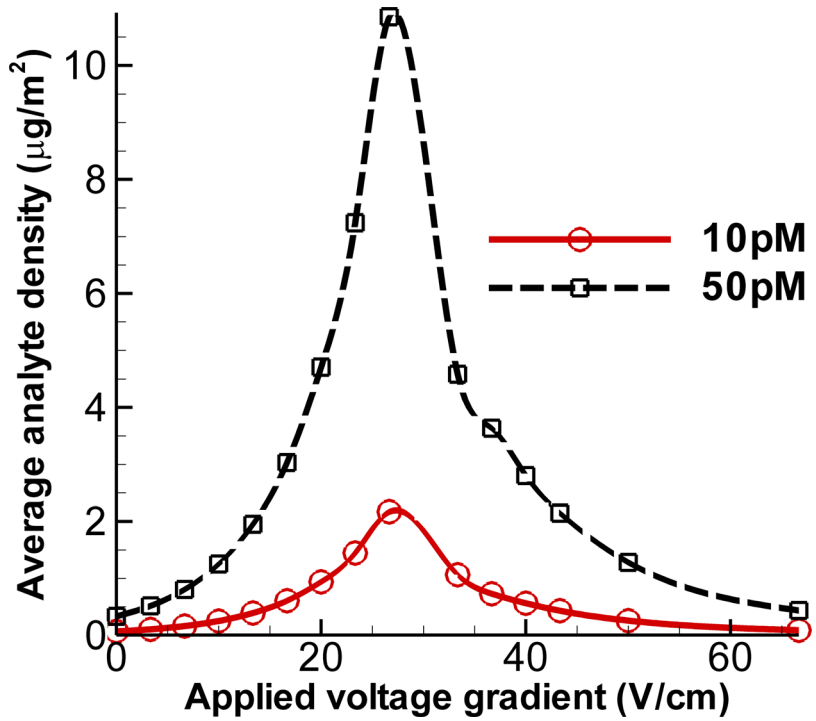

FIG. 6. The effect of applied voltage gradient on average analyte surface density at steady state.

Figure 7 shows the time evolutions of the frequency down shift induced by the analyte deposition to the micro resonator surface. The frequency down shift curve reflects the detection of a real WGM sensor. Two different cases are shown. The applied voltage gradients are set to be

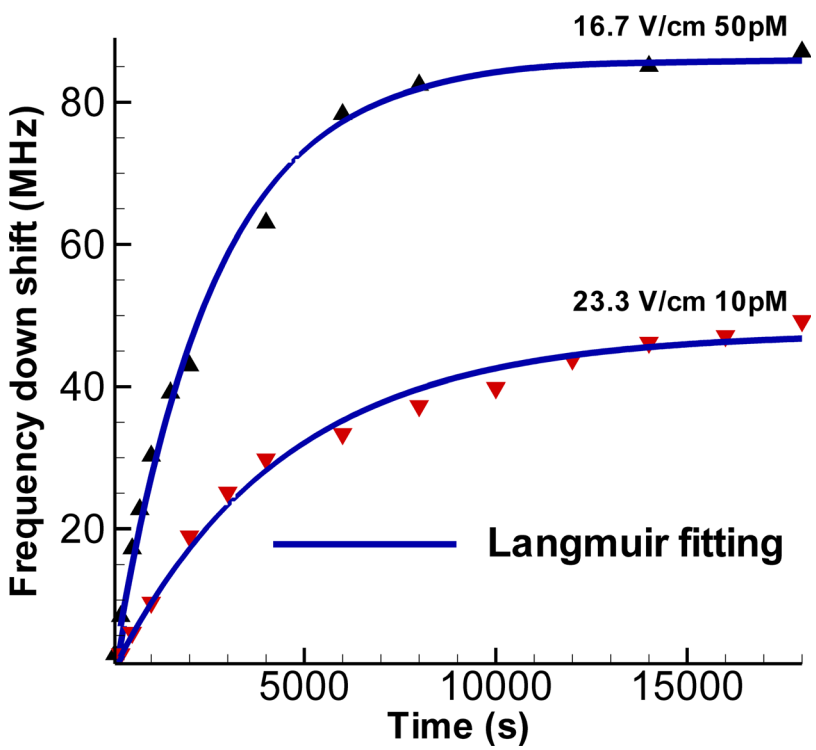

FIG. 7. The time trace of frequency down shift induced by analyte deposition onto the sensor surface.

TABLE II. Comparison of time constants between the adsorption kinetics and frequency shift fitting.

$\nabla\Phi$ (V/cm)	C_1 (pM)	τ_1 (s)	τ_2 (s)	$\lvert(\tau_2-\tau_1)\rvert/\tau_1\times 100\%$
6.67	10	1963	1979	0.8
	50	1481	1468	0.9
16.7	10	3337	3308	0.8
	50	2598	2616	0.7
23.3	10	4298	4450	3.5
	50	4222	4125	2.3

16.7 and 23.3 V/cm with corresponding analyte feed concentrations of 50 and 10 pM, respectively. Via the Langmuir fitting, the time constant τ for the case of 16.7 V/cm and 50 pM is found to be 2616 s, and that for the case of 23.3 V/cm and 10 pM is 4450 s.

Table II compares the time constants obtained through the adsorption kinetics (τ_1) and the frequency shift data (τ_2), respectively. The difference between these two constants for the cases studied is small. It verifies that the time trace of the adsorption process can be accurately monitored by the detection of the WGM frequency shift.

Figure 8 shows the relationship between the detected frequency down shift and the analyte concentration at steady state. It is seen that the shift increases with increasing analyte concentration and increasing applied voltage gradient. Using the best fitting technique, a sensor curve equation is obtained as $\Delta f(\mathrm{MHz}) = -(0.2433 + 0.00053 \times \nabla\Phi(\mathrm{V/cm})^{2.85}) \times C_1(\mathrm{pM})$. The correlation shows a linear relationship between the concentration and the frequency shift and a power function of the potential gradient. The external electrical field enhances the adsorption in the controlled applied voltage range. The results demonstrate the feasibility of the proposed WGM-MOEFS biosensor as an excellent miniature platform for monitoring bio-molecules of very low concentrations. This new biosensing system can be utilized for analysis of low-concentration analyte as well as for the study of dynamic adsorption processes.

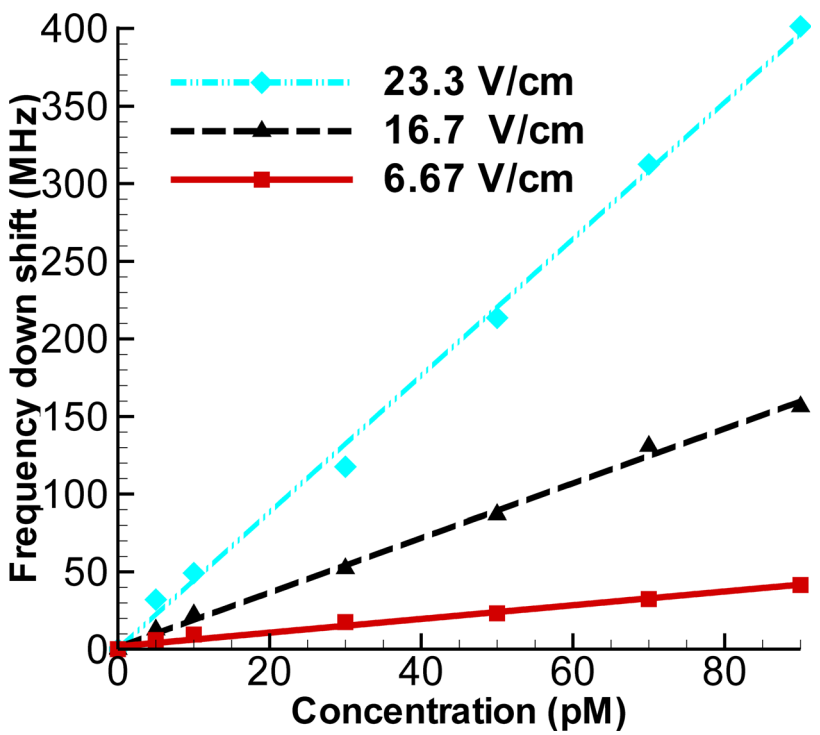

FIG. 8. The resonance frequency shift versus the analyte feed concentration for different applied voltage gradients at steady state.

The increase of temperature in the sensor due to Joule heating is found to be in the order of μK because of the extremely low concentration of charged ions and analytes in the neutral solution. A temperature induced resonance frequency shift can be analyzed as

$$-\frac{\Delta f}{f}=\frac{\Delta n_{eff}}{n_{eff}}+\frac{\Delta r}{r}=-\left[\frac{\eta n_m\beta_m+(1-\eta)n_s\beta_s}{n_{eff}}+\alpha_m\right]\Delta T, \tag{21}$$

where Δf represents the frequency shift; f indicates the base frequency; r is the radius of the micro resonator; α and β are the thermal expansion coefficient and thermo-optic coefficient, respectively; η is the radiation confinement factor; and n_{eff} indicates the effective refractive index of the propagating mode inside the micro resonator. Subscripts m and s represent the micro resonator and the surrounding solution, respectively. In the current situation, $\alpha_m=3.3\times10^{-6}$ K^{-1}, $\beta_m=2\times10^{-5}$ K^{-1} and $\beta_s=-16.5\times10^{-5}$ K^{-1} at 300 K, and η is 80–90%. The frequency down shift induced by 1 μK temperature rise is analyzed as about 2.3 kHz, which is negligible as compared to the frequency shift (in the order of MHz) induced by analyte deposition.

IV. CONCLUSION

Integration of the optical WGM and microelectrofluidic system brings in a new compact MOEFS device for biological sensing and chemical analysis. In this system, the analyte is directed to the WGM biosensor through a microchannel flow under the effect of an externally applied electric field. The adsorption process and analyte concentration are traced by measuring the WGM resonance frequency shift. The whole charged species manipulation and detection processes, including the species transport in the microchannel, adsorption and desorption processes on the surface of the resonator, and the whispering-gallery mode optical resonances, were simulated via the finite element method.

The temperature change of the micro resonator due to Joule heating is very small in the considered applied voltage range because of the extremely low ions concentration in the neutral solution. Its induced resonance frequency shift is negligible as compared with induced shift by analyte deposition. The analyte adsorption process on the micro resonator surface can be accurately monitored by tracking the frequency shift over time. The simulated curves fit into the Langmuir-like adsorption kinetics. The time constant for the dynamic adsorption process can be obtained from the frequency shift curve.

A correlation of the frequency shift, the analyte concentration in the solution, and the applied voltage gradient was obtained, which revealed a linear relationship between the analyte concentration and the resonance frequency shift. The applied voltage gradient was found to influence the adsorption capability. With increasing applied voltage gradient, both the analyte density on the sensor surface and the sensor sensitivity increase. The simulated WGM sensor is found to function at very low analyte concentrations, down to the pico-molar concentration level.

ACKNOWLEDGMENTS

This material is based upon work supported by a USDA NRI competitive grants program award, 2008-01336, and partially supported by a Charles and Johanna Busch Memorial Fund award for biomedical research.

[1]J. Emmelkamp, F. Wolbers, H. Andersson, R. S. DaCosta, B. C. Wilson, I. Vermes, and A. V. D. Berg, Electrophoresis **25**, 3740 (2004).
[2]A. C. Romano, E. M. Espana, S. H. Yoo, M. T. Budak, J. M. Wolosin, and S. C. G. Tseng, Invest. Ophthalmol. Vis. Sci. **44**, 5125 (2003).
[3]S. Arnold, M. Khoshsima, I. Teraoka, S. Holler, and F. Vollmer, Opt. Lett. **28**, 272 (2003).
[4]T. Endo, K. Kerman, N. Nagatani, Y. Takamura, and E. Tamiya, Anal. Chem. **77**, 6976 (2005).
[5]H. Shao, D. Kumar, and K. L. Lear, IEEE Sens. J. **6**, 1543 (2006).
[6]A. Q. Liu, H. J. Huang, L. K. Chin, Y. F. Yu, and X. C. Li, Anal. Bioanal. Chem. **391**, 2443 (2008).
[7]Z. Guo, S. Maruyama, and A. Komiya, J. Phys. D: Appl. Phys. **32**, 995 (1999).
[8]S. A. Leung, R. F. Winkle, R. C. R. Wootton, and A. J. D. Mello, Analyst (Cambridge, U.K.) **130**, 46 (2005).
[9]X. Cui, X. Heng, J. Wu, Z. Yaqoob, A. Scherer, D. Psaltis, and C. Yang, Opt. Lett. **31**, 3161 (2006).

[10]T. P. Burg, M. Godin, S. M. Knudsen, W. Shen, G. Carlson, J. S. Foster, K. Babcock, and S. R. Manalis, Nature **446**, 1066 (2007).
[11]Y. Sun, C. S. Lim, A. Q. Liu, T. C. Ayi, and P. H. Yap, Sens. Actuators A **133**, 340 (2007).
[12]F. Vollmer, D. Braun, A. Libchaber, M. Khoshsima, I. Teraoka, and S. Arnold, Appl. Phys. Lett. **80**, 4057 (2002).
[13]H. Quan and Z. Guo, J. Quant. Spectrosc. Radiat. Transf. **93**, 231 (2005).
[14]H. Quan and Z. Guo, Nanotechnology **18**, 375702 (2007).
[15]F. Vollmer and S. Arnold, Nat. Methods **5**, 591 (2008).
[16]M. Gorodetsky, A. Savchenkov, and V. Ilchenko, Opt. Lett. **21**, 453 (1996).
[17]M. Sumetsky, R. Windeler, Y. Dulashko, and X. Fan, Opt. Express **15**, 14376 (2007).
[18]T. Ioppolo, N. Das, and M.V. Ötügen, J. Appl. Phys. **107**, 103105 (2010).
[19]T. Carmon, L. Yang, and K. Vahala, Opt. Express **12**, 4742 (2004).
[20]Q. Ma, T. Rossmann, and Z. Guo, J. Phys. D: Appl. Phys. **41**, 245111 (2008).
[21]Q. Ma, T. Rossmann, and Z. Guo, Meas. Sci. Technol. **21**, 025310 (2010).
[22]H. Lin, D. B. Storey, H. O. Michael, C. H. Chen, and J. G. Santiago, Phys. Fluids **16**, 1922 (2004).
[23]J. D. Jackson, *Classical Electrodynamics* (Wiley, New York, 1998).
[24]K. L. Jones and C. R. O'Melia, J. Membr. Sci. **165**, 31 (2000).
[25]S. Mezzasalma, D. Baldovino, J. Colloid Interface Sci. **180**, 413 (1996).
[26]http://en.wikipedia.org/wiki/Bovine_serum_albumin.
[27]M. A. Brusatori, Y. Tie, and P. R. van Tassel, Langmuir **19**, 5089 (2003).
[28]K. Yeung, Z. Lu, and N. Cheung, Colloids Surf., B **69**, 246 (2009).
[29]S. Karpov and I. Krichtafovitch, in *Proceedings of the comsol Multiphysics User's Conference*, Boston, USA, 23–25 October 2005.
[30]Z. M. Wu and D. Q. Li, Electrochimica Acta. **53**, 5827 (2008).
[31]K. C. Kwok, K. M. Yeung, and N. H. Cheung, Langmuir **23**, 1948 (2007).
[32]B. H. Crichto, H. Li, and R. A. Fouracre, in *Proceedings of 6th International Conference on Dielectric Materials, Measurements and Applications*, IEEE, Manchester, UK, 7–10 September 1992.
[33]R. Kurrat, J. Prenosil, and J. Ramsden, J. Colloid Interface Sci. **185**, 1 (1997).
[34]E. Samson, J. Marchand, and K. A. Snyder, Mater. Struct. **36**, 156 (2003).